

Energy Landscape analysis of metal-insulator transitions: theory and application to Ca_2RuO_4 , RNiO_3 and their heterostructures

Alexandru B. Georgescu^{1,2} and Andrew J. Millis^{2,3}

¹Northwestern University, Department of Materials Science and Engineering, Evanston, Illinois, 60208

²Center for Computational Quantum Physics, Flatiron Institute, 162 5th Avenue, New York, NY 10010*

³Department of Physics, Columbia University, 538 West 120th Street, New York, New York 10027

(Dated: May 7, 2021)

We present a general methodology that enables the disentanglement of the electronic and lattice contributions to the metal-insulator transition by building an energy landscape from numerical solutions of the equation of state. The methodology works with any electronic structure method that provides electronic expectation values at given atomic positions. Applying the theory to rare-earth perovskite nickelates (RNiO_3) and Ruddlesden-Popper calcium ruthenates (Ca_2RuO_4) in bulk, heterostructure and epitaxially strained thin film forms using equation of state results from density functional plus dynamical mean field calculations we show that the electron-lattice coupling is an essential driver of the transition from the metallic to the insulating state in these materials.

I. INTRODUCTION

The relative importance of electronic and lattice effects in driving phase transitions in quantum materials is a subject of long-standing interest and controversy. One issue of particular focus is the metal to insulator transition (MIT), which in many materials is accompanied by a lattice distortion [1]. Multiple studies have addressed various aspects of the interplay between electronic and lattice contributions to the metal-insulator transition both theoretically and experimentally [2–48]. Machine learning approaches are discovering new features from comparison of MIT and non-MIT materials [49, 50]. Yet, the relative importance of electronic and lattice effects in producing a transition has remained unclear, in part because of the lack of an appropriate theoretical framework and computational schema for evaluating the needed quantities. This paper aims to rectify both issues.

Metal insulator transition phenomena are properly analysed by constructing an energy landscape in the space of lattice distortions and electronic orders such as that shown in Fig. 1. We show how to build these energy landscapes from numerical data of the kind now available from modern quantum many-body methods and we apply the theory to bulk, thin film and superlattice heterostructures of RNiO_3 and Ca_2RuO_4 , two material families that exhibit metal-insulator transitions but have different local physics.

Our work was inspired by the pioneering work of Fisher and collaborators [51], who combined elegant experimental measurements with an insightful free energy analysis to show that the observed second order ‘nematic’ transition in an iron pnictide material had an intrinsically electronic origin. Our work may be viewed as a generalization of the ideas of Fisher et. al to first order transitions, where a more global view of the energy landscape is required, and as an extension of the insightful equation of state analysis

of Peil, Hampel, Ederer and Georges [4] to the computation and interpretation of the full free energy landscape. We make substantial use of concepts put forward in analyses of the metal-insulator transition in epitaxially strained Ca_2RuO_4 [7] and in nickelate heterostructures [3].

The rest of this paper is organized as follows: the Framework section (II) shows how we build total energy landscapes. In sections III and IV we use the formalism to analyse the metal-insulator transitions occurring in two representative classes of materials: the rare earth nickelate perovskite RNiO_3 compounds, where the transition involves a symmetry breaking lattice distortion and two sublattice electronic ‘charge order’ and Ca_2RuO_4 where the transition is isostructural (no structural symmetry breaking) and involves electronic ‘orbital order’. Section

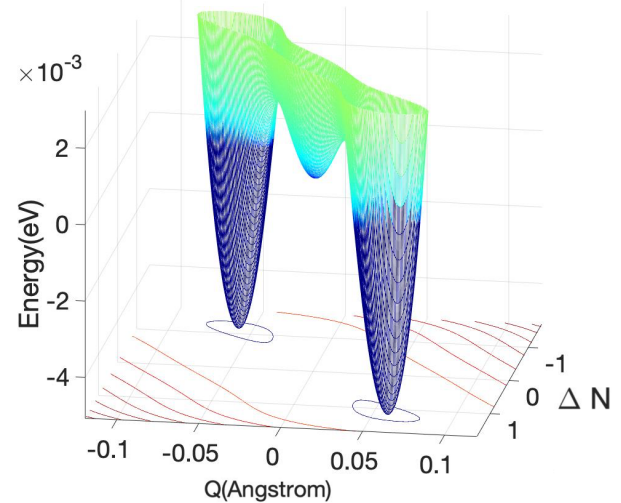


FIG. 1: Energy landscape for NdNiO_3 as a function of electronic charge disproportionation ΔN and lattice distortion Q as obtained from the energy functional methods introduced in this paper using data from Ref. [3].

* alexandru.georgescu@northwestern.edu

V presents some qualitative considerations related to the thermally driven transitions. Section VI is a summary and conclusion, assessing the work and outlining future directions.

II. FRAMEWORK

Following Refs. [3, 4, 7] we consider a free energy $F(\Delta N, Q)$ that depends on an electronic order parameter, ΔN , and a lattice distortion, Q . The precise definitions of ΔN and Q will depend on the specifics of the system. We choose $(Q, \Delta N) = (0, 0)$ as the equilibrium configuration of the metallic phase. The insulating state then corresponds to a configuration $(\Delta N, Q) \neq (0, 0)$ and the question of the existence of a purely electronic transition relates to the properties of F as a function of ΔN at $Q = 0$.

A second order transition corresponds to a linear instability of the $(\Delta N, Q) = (0, 0)$ state, in other words to a change in sign of the smallest eigenvalue of the Hessian matrix $\partial^2 F / \partial^2 \Delta N, Q$ evaluated at $\Delta N = Q = 0$. In general the eigenvector associated with the negative eigenvalue will have components along both ΔN and Q , indicating that the electronic and lattice orders are coupled. A purely electronically driven transition would correspond to a change in sign of $\partial^2 F / \partial^2 \Delta N$, a lattice-driven transition would correspond to a change in sign of $\partial^2 F / \partial^2 Q$, and in a mixed situation neither ‘pure’ derivative changes sign but the lowest eigenvalue of the Hessian matrix does change sign. In the case of the nematic transition in pnictides, Fisher and co-workers were able [51] to experimentally determine $\partial^2 F(Q = 0) / \partial \Delta N^2$ and show that it changed sign at a temperature only slightly lower than the observed nematic transition temperature, thereby establishing that a purely electronically driven nematic transition exists in these materials, and is simply slightly enhanced by coupling to the lattice.

The transitions of interest in this paper are first order, characterized by the appearance of a new free energy minimum at which ΔN and Q are both different from zero (see e.g. Fig. 1). Study of first order transitions requires global knowledge of the free energy. One may say that the transition is electronically driven if $F(\Delta N, Q = 0)$ has an extremum at a $\Delta N \neq 0$ with $\partial^2 F(\Delta N, 0) / \partial \Delta N^2 > 0$ and with energy lower than $F(0, 0)$. One may say that the transition is lattice-assisted if $F(\Delta N, 0)$ has a local minimum at a $\Delta N \neq 0$ but that the lattice coupling is required to make this minimum the ground states. Finally if $F(\Delta N, Q = 0)$ has only one minimum, at $\Delta N = 0$ but exhibits a stable minimum with $\Delta N \neq 0$ at a $Q \neq 0$ then we may say that the transition is not electronically driven. The energy functional shown in Fig. 1 shows a transition that is not electronically driven because the global minima are at a $Q, \Delta N \neq 0$ but along the line $Q = 0$ the functional has only one minimum, at the origin. It is important to emphasize that this distinction is separate from the question of the importance of correlation physics.

It is common in the literature to distinguish strongly from weakly correlated materials according to whether or not current implementations of density functional theory capture the physics; in current language whether a density functional calculation of F_{el} suffices; even if the transition is not electronically driven in the sense given above, beyond density functional correlations might be needed to obtain an $F_{el}(\Delta N, Q)$ with an insulating minimum at the physical Q .

The global knowledge of F required to decide this issue has been challenging to obtain. Available quantum many-body methods can with reasonable computational cost obtain reasonable estimates of the optimal ΔN that minimizes F at fixed atomic positions (Q), but finding the dependence of F on ΔN at fixed Q or on Q at fixed ΔN is difficult, both because it is not straightforward to control ΔN independently of Q and because calculations of energies are very expensive.

Here we build on the observation that the metal-insulator transitions of greatest current experimental interest share two features that greatly simplify an analysis. First, the lattice energetics is to good approximation harmonic [3, 4, 7], as shown from calculations [3] and by the observation that phonon frequencies change only very slightly ($\sim 1\%$) across the metal-insulator transition. Second, and closely related to the first point, the coupling between the electronic order parameter and lattice modes is linear and is well determined by standard theoretical methods [3, 4, 7], as are the lattice energetics. This means that we may write, schematically, [3, 4, 7]:

$$F(\Delta N, Q) = \frac{1}{2} K Q^2 - \frac{1}{2} g Q \Delta N + F_{el}(\Delta N) \quad (1)$$

Requiring stationarity of F with respect to variations in ΔN and Q yields the equations of state [3, 4]

$$K Q = \frac{1}{2} g \Delta N \quad (2)$$

and

$$\frac{\partial F_{el}(\Delta N)}{\partial \Delta N} = \frac{1}{2} g Q \quad (3)$$

Because g and K are known, Eq. 2 can be solved. Substituting the solution back into Eq. 1 produces:

$$\bar{F}(\Delta N) = -\frac{1}{8K} (g \Delta N)^2 + F_{el}(\Delta N) \quad (4)$$

From this point of view the key question is the magnitude of the ‘lattice stabilization energy’ $\frac{1}{8K} (g \Delta N)^2$: is it large enough to create a new extremum at a $\Delta N \neq 0$? Is it large enough to ensure that the extremum at $\Delta N = 0$ is unstable? Answering this question requires knowledge of F_{el} .

Peil, Hampel, Ederer and Georges observed [4] that existing many-body methods such as the dynamical mean field method enable computation of electronic properties at fixed lattice configuration Q , in effect solving

Eq. 3. Here we take one further step: the ansatz for the electronic energy functional in Eq. 1 means that the computed $\Delta N(Q)$ determines $dF_{el}(\Delta N)/d\Delta N$; the derivative can then be integrated, thereby constructing F itself. In practice we perform the integration by fitting the $\Delta N(Q)$ results to a polynomial, which is analytically integrated. While this method requires a choice of polynomial form, we empirically find that the uncertainty thereby introduced is small, of the order of a few meV, comparable to the error in performing an explicit energy calculation. This approach is computationally inexpensive, relatively unaffected by noise, and the analytically specified functional forms provide additional insight, in particular enabling straightforward examination of the global energy landscape.

We use this approach to analyse the metal-insulator transitions occurring in the rare-earth nickelates and their heterostructures, and in bulk and epitaxially strained Ca_2RuO_4 . We find that in all of these situations the metal-insulator transition is, in the sense defined above, not electronically driven.

III. BULK RARE-EARTH NICKELATES

A. Materials and notation

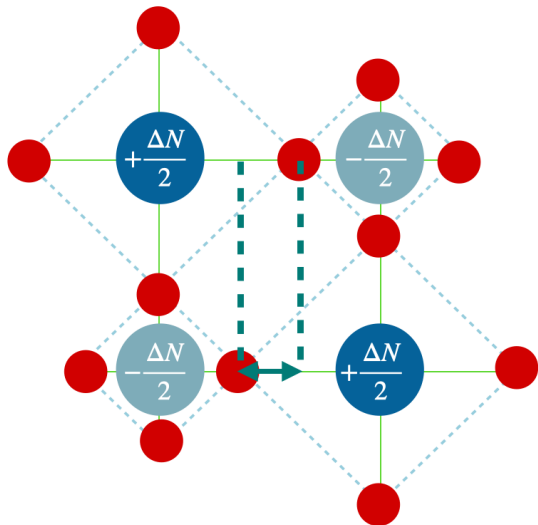


FIG. 2: Schematic of the electronic and structural disproportionation in the insulating state in rare-earth nickelates: NiO_6 octahedra disproportionate electronically and structurally in a checkerboard pattern.

In the low-energy model of Ref. [4], the Ni ions corresponding to the larger octahedra have $1e^- + \frac{\Delta N}{2}$ electrons in their e_g shell, while those corresponding to the smaller one have $1e^- - \frac{\Delta N}{2}$. The difference in average bond lengths defines Q for the nickelate materials.

The perovskite rare-earth nickelates have chemical

formula $R\text{NiO}_3$; when synthesized in bulk form the materials with $R=\text{Lu}, \text{Y}, \text{Sm}, \text{Nd}, \text{Pr}$ exhibit a first order transition from a high temperature metal to a low temperature insulator while LaNiO_3 remains metallic down to lowest temperature. The material properties depend systematically on the choice of rare-earth ion, with LuNiO_3 exhibiting the highest metal insulator transition temperature $T_{MIT} = 600\text{K}$, SmNiO_3 having $T_{MIT} \approx 400\text{K}$, NdNiO_3 having a $T_{MIT} \approx 240\text{K}$ and PrNiO_3 having a $T_{MIT} \approx 130\text{K}$ [11, 52, 53]. The materials may also be grown in heterostructure form [2, 3, 5, 11, 12, 18, 44, 54, 55], with a small number of layers of $R\text{NiO}_3$ sandwiched between layers of other materials. The metal-insulator transition temperature in the heterostructures differs from that in bulk.

Except for the La compound, where the symmetry is slightly different, the high temperature metallic state forms in a Pbnm structure which for present purposes may be regarded as a pseudo-cubic lattice of Ni ions with an O ion at the midpoint of each Ni-Ni bond. The insulating state is characterized by a two-sublattice bond disproportionation, with one Ni sublattice having a short mean Ni-O bond length and the other by a long one, represented qualitatively in Fig. 2. The difference in mean Ni-O bond lengths defines the lattice mode Q appropriate to this transition.

In the low T insulating state the two Ni sublattices differ in electronic configuration. This difference has been characterized in various ways in the literature. [4, 30, 39, 56–58]. We follow Peil and collaborators [4] and define the electronic change ΔN as the difference in the occupation of the e_g states obtained from a narrow window Wannier fit of the bands crossing the Fermi level.

B. Results, bulk nickelates

In Fig. 3 we present results for three different bulk-form rare earth nickelates, ($\text{LuNiO}_3, \text{SmNiO}_3, \text{PrNiO}_3$) as a function of Q , digitized from the calculations of ΔN presented in Ref. [4]. In all compounds, two regimes are found, a low Q regime where ΔN is proportional to Q and a high Q regime where ΔN is large but weakly dependent on Q ; the two regimes are separated by a discontinuity.

To determine the free energy model to which the results should be fit we observe that the two sublattice nature of the insulating state means that the free energy must be invariant under simultaneous inversion $Q \leftrightarrow -Q$, $\Delta N \leftrightarrow -\Delta N$, so in particular $F_{el}(\Delta N)$ must be even in ΔN . Motivated by the observed first order nature of the transition we assume that F_{el} is a 6th order polynomial in ΔN :

$$F_{el}(\Delta N) = \frac{1}{2}\chi_0^{-1}\Delta N^2 + \frac{1}{4}\beta\Delta N^4 + \frac{1}{6}\gamma\Delta N^6 \quad (5)$$

Solving Eq. 2 and eliminating Q from the full free energy then changes the quadratic term $\chi_0^{-1} \rightarrow \chi_0^{-1} - \frac{g^2}{4K}$.

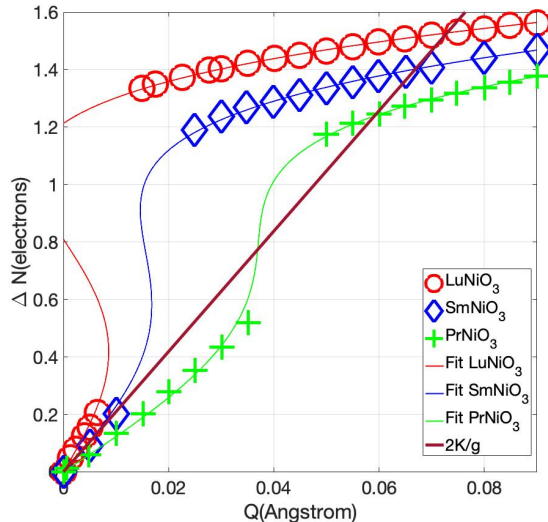


FIG. 3: Points: $\Delta N(Q)$ values used for the three $R\text{NiO}_3$ materials as obtained from DFT+DMFT calculations from Ref. [4]; Light lines: fits of the points to Eq. 6. Also shown is the $Q(\Delta N)$ line obtained from the Q equation of state Eq. 2. Note that K/g has the same value for all three materials.

Note that the shift in the quadratic term involves the parameter g^2/K , which varies slightly across the $R\text{NiO}_3$ series although as noted in Ref. [4] the ratio g/K is almost material-independent. The K for the Lu, Sm, Pr materials were reported in reference [4] to be 39.29, 41.45 and 44.47 eV/Å², while the g are 3.75, 4.02 and 4.24 eV/Å.

Eq. 5 implies that the equation of state Eq. 3 takes the explicit form

$$0 = -gQ + \chi_0^{-1}\Delta N + \beta\Delta N^3 + \gamma\Delta N^5 \quad (6)$$

We fit the points in Fig. 3 to Eq. 6, using the g values presented in Ref. [4], obtaining the light solid curves shown in Fig 3 and the fit parameters given Table I. It is important to note that the DMFT equation of state shown in Fig. 3 has two branches, with the solution discontinuously changing from one to the other as Q is varied. In our fits we only use the data points shown as symbols in Fig. 3; these points lie outside the region of multistability (i.e. where two ΔN solutions exist within DMFT for the same Q). However, our theoretical energy function reproduces correctly behavior that was not part of the original fit, for example the locally stable large ΔN at $Q = 0$ solution for LuNiO_3 [4]. Including points within the region of multistability does not lead to significant changes to our results. The free energy we obtain here may be thought of as the free energy that would be obtained from the two component Landau theory of Ref. [4] if the metal-insulator variable is integrated out.

$R\text{NiO}_3$	χ_0^{-1} (eV)	β (eV)	γ (eV)	$-\frac{1}{4}\frac{g^2}{K}$ (eV)
LuNiO_3	0.0596	-0.1314	0.0618	-0.0895
SmNiO_3	0.0945	-0.1303	0.0667	-0.0975
PrNiO_3	0.1749	-0.1713	0.0804	-0.1011

TABLE I: Parameters that characterize the electronic and total energy of the three $R\text{NiO}_3$ materials, as extracted by fitting the data from Ref [4] to Eq. 6.

The left panel of Fig. 4 shows the purely electronic energy F_{el} corresponding to the fit parameters given in Table I. We see that for all of the materials the purely electronic theory is characterized by a locally and globally stable metallic minimum at $Q = 0$. Only for LuNiO_3 does a second, insulating extremum exist and even in this case it is not energetically favored. The central panel presents the total free energy as a function of ΔN obtained by minimization over the lattice degrees of freedom Q . We see that inclusion of the lattice coupling is necessary to stabilize the $\Delta N, Q \neq 0$ solution: in other words, it is the electron-lattice coupling that drives the transition.

Table I shows that as one moves across the $R\text{NiO}_3$ series from $R=\text{Lu}$ (most insulating) to $R=\text{Pr}$ (least insulating), the linear response electronic susceptibility of the metallic state decreases, consistent with the empirical observation that the Lu material is the strongest insulator and the Pr material is the weakest. We see also that the nonlinear terms in the energy are the same for the Lu and Sm compounds, which are the two strong insulators, but are different in the Pr compound, which is close to the metal-insulator transition. To understand composition-dependent changes one must consider more than just the variation in linear response susceptibilities. Results to be presented below for superlattices further confirm this point.

The present theory predicts that PrNiO_3 is undistorted and metallic, although close to the metal-insulator transition boundary, while the compound is empirically distorted and insulating, although again with a very low transition temperature. We believe this discrepancy arises because the transition in PrNiO_3 is from a paramagnetic metal to an antiferromagnetic insulator, in contrast to the Sm and Lu materials where the transition is between two paramagnetic phases. Inclusion of antiferromagnetism in the theory will yield a lower energy for the insulating phase of PrNiO_3 at the U, J values used here while a slightly different choice of interaction parameters would also push PrNiO_3 to the insulating side of the phase diagram.

We may take the analysis further by substituting the $\Delta N(Q)$ obtained from the solution of Eq. 6 into the full free energy expression to obtain the free energy as a function of the lattice coordinate Q shown in the right panel of Fig. 4. This is analogous to the energy that is usually calculated by electronic structure codes, which work at fixed atomic positions. The discontinuities arise from the different branches of the $\Delta N(Q)$ curves. The resulting

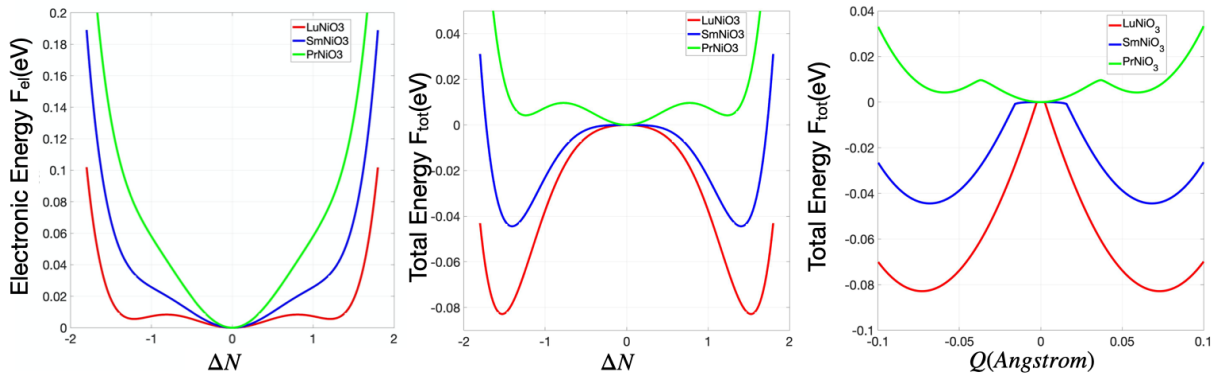


FIG. 4: Left panel: electronic energy; central panel: total energy of three RNiO₃ compounds as function of electronic order parameter ΔN . Right panel: total energy as function of lattice displacement Q .

free energy is, to a good approximation, the combination of two parabolic energy curves, one corresponding to the metallic state, and one to the insulating state. We see that in this theory the $\Delta N = 0$, $Q = 0$ state is stable to lattice distortions for PrNiO₃, marginally stable for SmNiO₃ and unstable for LuNiO₃.

The analysis presented here is based on a fit of the computed $\Delta N(Q)$ to a free energy model. We emphasize that this fit is in no way essential to our method; one could simply numerically integrate a suitably dense set of $\Delta N(Q)$ data. But for the procedure used here the question of the sensitivity of the results to the choice of free energy arises. To quantify the uncertainties we have refit the PrNiO₃ data shown in Fig. 3, now constraining the 4th and 6th order coefficients to have the same values as found in SmNiO₃. Results are shown in Fig 5. We

see from the left panel that this fit to the data is not quite as good, especially in the small to intermediate Q region. The fitted energy (right panel) is very similar to that shown in Fig. 4, with the value of ΔN at the minimum almost the same in the two cases and the energy of insulating solution in the constrained fit is now slightly lower than the energy of the metallic solution, placing paramagnetic PrNiO₃ slightly on the insulating side of the transition. These differences indicate that the systematic uncertainties in the method are not large.

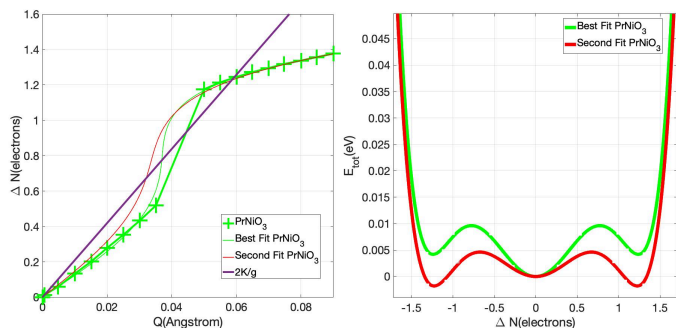


FIG. 5: Fits and total energy for PrNiO₃ based on DMFT data from Ref [4]; green lines correspond to the optimal polynomial fit, red lines to 4th and 6th kept constant to the values extracted for SmNiO₃, and only the quadratic term fitted to the data.

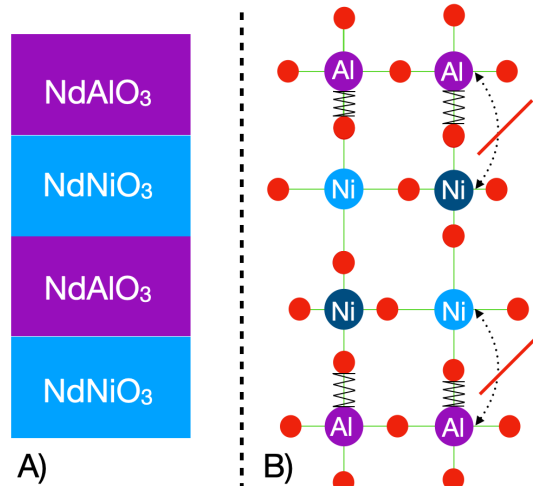


FIG. 6: a) Schematic of superlattice consisting of NdNiO₃ layered in between the band insulator NdAlO₃ b) Schematic view of two atomic layers of NdNiO₃ sandwiched between NdAlO₃ layers as described in reference [3]. Dashed line with red slash: forbidden hopping path, indicating mechanism of dimensional reduction. Zig-zag lines connecting O and Al: representation of increased stiffness to distortions of the Al-O bonds relative to the Ni-O bonds.

C. Layered Structures of NdNiO₃/NdAlO₃

An important modern direction in quantum materials science is heterostructuring: the ability to synthesize structures in which atomically thin planes of one material alternate with atomically thin planes of another. Previous experimental [5] and theoretical [3] work analysed systems of the type shown schematically in Fig. 6 in which a few layers of metal-insulator transition compound NdNiO₃ were grown as a thin film sandwiched epitaxially between layers of the wide-gap insulator NdAlO₃. The few-layer systems had significantly higher transition temperatures than did bulk NdNiO₃. Theoretical DFT+DMFT results are available [3] for three systems: bulk NdNiO₃ and two heterostructured systems with a 4 unit cell repeat distance: one layer of NdNiO₃ followed by three of NdAlO₃ ("monolayer"), and two layers of NdNiO₃ followed by two of NdAlO₃ ("bilayer"). The $\Delta N(Q)$ results are shown in Fig. 8

Two competing effects were found [3]: the electronic confinement of the electrons in the NdNiO₃ by the nearby NdAlO₃ layers favors a higher electronic disproportionation ΔN , while the energy cost of imposing a lattice distortion on the adjacent Al-O octahedra is equivalent to an increase in the stiffness K of the NiO₆ lattice with a $K=31.6914\text{eV}/\text{\AA}^2$, for the bulk material, $K=35.6269\text{eV}/\text{\AA}^2$ for the bilayer and $K=40.4753\text{eV}/\text{\AA}^2$ for the monolayer; all energies per 10 atom unit cell. The values for g are those quoted in [3]; we reproduce them here for convenience: $g = 3.2212\text{eV}/\text{\AA}$ for the bulk, $g = 3.3465\text{eV}/\text{\AA}$ for the bilayer and $g = 3.3780\text{eV}/\text{\AA}$ for the monolayer. Performing an analysis similar to that presented in Sec. III leads to the energy curves presented in Fig. 7 and to the fit parameters shown in Table II. The original data with the fit are presented for convenience in Fig. 8

Turning first to the purely electronic correlation energy shown in the left panel of Fig. 7, we observe that neither NdNiO₃ nor the heterostructured materials show a purely electronically driven insulating state; however, hints of an inflection point, the precursor of the formation of a higher ΔN extremum, can be seen in bilayer and monolayer curves around $\Delta N = 1$ reflecting the effect of quantum confinement in increasing the electron correlations. Inclusion of the lattice energy produces a global, insulating minimum in all three materials. The monolayer and bilayer show a significantly larger energy difference between the insulating and the metallic states than does bulk NdNiO₃, in agreement with their higher T_{MIT} .

The origin of the effect is surprising: the modest decrease in the magnitude of g^2/K as we pass from bulk to bilayer to monolayer reflects the increase in lattice stiffness, opposing the order, and nearly counterbalances the modest decrease in χ_0^{-1} reflecting the increased correlation physics of the confined metallic state. The more important effect, however, is the change in the magnitude

Layers	$\chi_0^{-1}(\text{eV})$	$\beta(\text{eV})$	$\gamma(\text{eV})$	$-\frac{1}{4}\frac{g^2}{K}(\text{eV})$
Bulk	0.1049	-0.1022	0.0631	-0.0819
Bilayer	0.0823	-0.0879	0.0545	-0.0789
Monolayer	0.0818	-0.0747	0.0377	-0.0705

TABLE II: Parameters that characterize the electronic and total energy of NdNiO₃ and NdNiO₃/NdAlO₃ heterostructures consisting of a single or two layers of NdNiO₃ from Ref [3].

of the higher order ($\Delta N^4, \Delta N^6$) terms shown in Table II. The change can be seen in Fig. 8 from the variation of the critical Q below which the insulating state is not stable. In the calculations presented in the previous subsection the higher order terms were also found to be different in PrNiO₃ (proximal to the metal-insulator transition) than in LuNiO₃ and SmNiO₃ (farther from the transition point).

IV. Ca₂RuO₄

A. Materials and Notation

Ca₂RuO₄ forms in a slightly distorted version of the $n = 1$ Ruddlesden-Popper structure, a layered structure consisting of RuO₂ planes separated by pairs of CaO layers. Each Ru is six-fold coordinated by oxygen, forming RuO₆ octahedra. The relevant electronic states (actually Ru-O hybrids) may be thought of as Ru t_{2g} symmetry d-states (d_{xy}, d_{xz}, d_{yz}) with 4 t_{2g} electrons per Ru. Below 340K the material undergoes a first-order transition from a high temperature metallic to a low temperature insulating phase. No symmetry is broken at the transition: the two phases share the same crystal structure but differ in the occupancies of the d orbitals and shape of the RuO₆ octahedra, and the relative occupancies of the d-levels. As sketched in Fig. 9, the metallic state is characterized by an approximately equal occupancy of the t_{2g} orbitals while in the insulating state the xy orbitals are doubly occupied and the xz/yz orbitals each contain a single electron. The appropriate electronic order parameter is the occupancy difference between the xy and xz/yz orbitals

$$\Delta N = n_{xy} - \frac{1}{2}(n_{xz} + n_{yz}). \quad (7)$$

No crystal symmetry protects the orbital occupancies in the high temperature metallic state, which is characterized by a $\Delta N = N_H$ close to, but not exactly, zero.

The change in electron occupancy across the metal-insulator transition occurs simultaneously with a decrease in the Ru-O apical bond length and an increase in the in-plane Ru-O bond length (a flattening of the octahedra). At the transition, there is a change in the lattice constants, and rearrangements of other internal coordinates. The harmonic nature of the lattice Hamiltonian means that most of the lattice modes may be integrated out, leaving

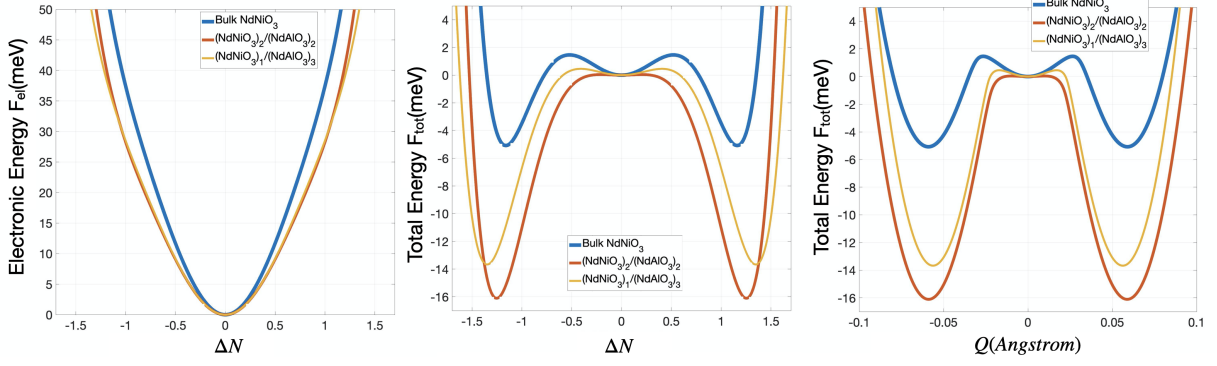


FIG. 7: Electronic (left panel) and total energy (central panel) as functions of electronic order parameter ΔN for bulk NdNiO_3 and for superlattices consisting of a bilayer of NdNiO_3 alternating with NdAlO_3 and a monolayer of NdNiO_3 alternating with 3 layers of NdAlO_3 using data from Ref. [3]. Right panel: total energy as function of lattice coordinate Q after minimizing over ΔN . Note change of y-axis scale between left-most and other two panels.

an effective theory involving two structural degrees of freedom. The two lattice degrees of freedom are needed, because if the point symmetry of the Ru ion is lower than cubic, then both the unit cell volume change and the relative octahedral distortion couple linearly to the differential level occupancy ΔN .

Following Ref. [7] we write the two relevant structural degrees of freedom as a variable Q_3 parametrizing a volume preserving change in the c-direction Ru-O bonds relative to the average in-plane Ru-O bonds, and a change Q_0 in the octahedral volume and define the lattice variables such that in the high-T metallic state $Q_3 = Q_0 = 0$. In terms of changes $\delta x, \delta y, \delta z$ to the three Ru-O bond lengths, defined as:

$$Q_0 = \frac{1}{\sqrt{3}}(\delta x + \delta y + \delta z) \quad Q_3 = \frac{1}{\sqrt{6}}(2\delta z - \delta x - \delta y) \quad (8)$$

We now build the free energy. We define the lattice distortion relative to the high-T metallic state as the

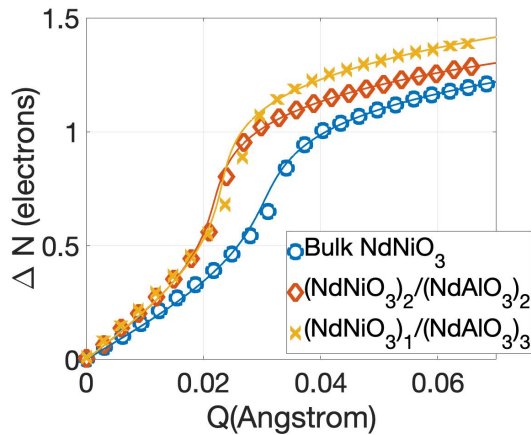


FIG. 8: Data from [3] (points) and the polynomials (light lines) obtained by fitting the data to the equation of state, Eq. 6

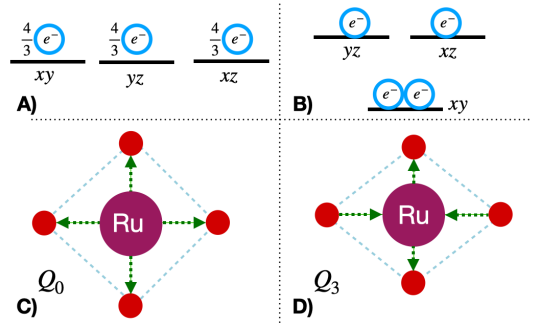


FIG. 9: Schematic of the electronic and structural disproportionation characterizing the metal-insulator transition of Ca_2RuO_4 . A) In the metallic phase, all 3 t_{2g} orbitals of Ca_2RuO_4 are approximately equally occupied; $\Delta N \approx 0$. B) In the insulating phase, the xy orbital is doubly occupied, while the yz and xz are singly occupied; $\Delta N = 1$ C) Representation of Q_0 structural mode, in which all bond lengths change equally D) Representation of structural mode Q_3 in which octahedral volume is preserved and the change in the two in-plane Ru-O bond lengths are equal, and opposite in sign to the change in the apical bond length. The electronic state in B) is associated with a structural term of the form $-(Q_3 - \lambda_0 Q_0)$, with $\lambda_0 > 0$

Representation of structural mode Q_3 in which octahedral volume is preserved and the change in the two in-plane Ru-O bond lengths are equal, and opposite in sign to the change in the apical bond length. The electronic state in B) is associated with a structural term of the form $-(Q_3 - \lambda_0 Q_0)$, with $\lambda_0 > 0$

vector $\vec{Q} = (Q_3, Q_0)$; the lattice restoring term \mathbf{K} is a 2×2 matrix with entries determined in previous work[7] to be $K_{33}=17.7$, $K_{03}=7.6$, $K_{00}=46.2$ eV/ \AA^2 per formula unit. We write the linear combination of the \mathbf{Q} that couples to the electronic disproportionation as $\vec{F} \cdot \vec{Q}$ with $\vec{F} = F_3(1, -\lambda)$. Ref. [7] finds $F_3 = 2.8\text{eV}/\text{\AA}$ and $\lambda = 0.45$.

$$F(\Delta N, Q) = \frac{1}{2} \mathbf{Q}^T \mathbf{K} \mathbf{Q} - \vec{F} \cdot \vec{Q} (\Delta N - \Delta N_H) + F_{el}(\Delta N), \quad (9)$$

Here ΔN_H is the value of ΔN in the high temperature insulating phase; it is nearly, but not quite, zero.

For the purely electronic energy we chose the 4th order form:

$$F_{el} = \frac{c\Delta N^4}{4} + \frac{b\Delta N^3}{3} + \frac{a\Delta N^2}{2} + \sigma_0\Delta N \quad (10)$$

Odd powers occur because no symmetry is broken at the transition.

B. Metal-insulator transition in bulk CaRuO₄

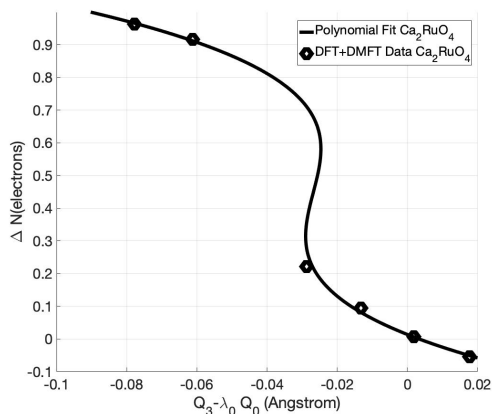


FIG. 10: $\Delta N(Q)$ from [7] (heavy black points) and polynomial fit (solid line) used for the equation of state.

Fig. 10 shows previously published results [7] for ΔN as a function of the relevant combination of lattice distortions along with our fit to Eq. 10. As in the previous section we have not used points in the coexistence region for the fit. We find $\sigma_0 = -0.009$, $a = 0.70$, $b = -1.718$, $c = 1.28$.

The higher curve (blue) in Fig. 11 shows the purely electronic free energy resulting from the fit. We see that in the absence of lattice effects the metallic, undistorted state is energetically favored and that there is not even a metastable minimum corresponding to the insulating state although there is a hint of an inflection point that is a precursor of a higher ΔN extremum. The lower trace (heavy black on-line) shows \bar{F} , the full free energy after the lattice modes has been integrated out. We see that inclusion of the lattice energetics qualitatively changes the free energy, strongly favoring large ΔN . Indeed we see that the energy does not have a minimum in the physically allowed range $\Delta N \leq 1$; rather it is minimized at the boundary $\Delta N = 1$. We again conclude that the transition in this compound is driven by the lattice contribution to the energetics.

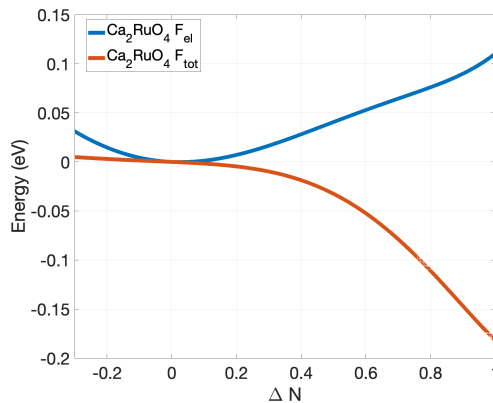


FIG. 11: $F_{el}(\Delta N)$ and $F_{total}(\Delta N)$ for Ca₂RuO₄.

C. Epitaxially constrained Ca₂RuO₄

Ca₂RuO₄ has also been grown epitaxially on insulating substrates. The epitaxial constraint means that the in-plane lattice parameters of the Ca₂RuO₄ are forced to be equal to the in-plane lattice parameters of the substrate material. *A priori*, this constraint does not fix the values of internal coordinates including the the Ru-O in-plane bond length of relevance here. Density functional theory calculations, however, [7] indicate that in practice the material adapts to the epitaxial constraint by adjusting the in-plane Ru-O bond lengths, rather than by rotating the Ru-O₆ octahedra, so that the percentage change in the in-plane Ru-O bond lengths is fixed by the percentage change in the in-plane lattice parameters. The z-direction lattice constants and Ru-O apical bond lengths are still of course free to relax. This means that the theory of the previous section can be simply adapted to the epitaxial case by a change of variables. We write:

$$Q_3 = \frac{1}{\sqrt{6}}(2z - x_0 - y_0) \quad (11)$$

and

$$Q_0 = \frac{1}{3}(z + x_0 + y_0) \quad (12)$$

with x_0 and y_0 fixed by the epitaxial constraint. It is also convenient to define the zero of z to be the value

$$z_0 = -(x_0 + y_0) \frac{K_{00} - K_{33} + \frac{K_{30}}{\sqrt{2}}}{2K_{33} + 2\sqrt{2}K_{30} + K_{00}} \quad (13)$$

that z would take at $\Delta N = N_H$.

We obtain:

$$F(\Delta N, z) = \frac{K'}{2}z^2 + g'(z - z^*)\Delta N + F_{el}(\Delta N) \quad (14)$$

with

$$K' = \frac{2}{3}(K_{33} + \sqrt{2}K_{30} + \frac{1}{2}K_{00}) \quad (15)$$

$$g' = \frac{F_3(2 - \sqrt{2}\lambda_0)}{\sqrt{6}} \quad (16)$$

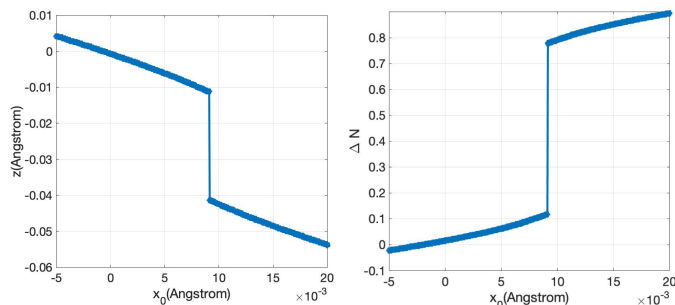


FIG. 12: Equilibrium ΔN and z versus epitaxial strain defined as the difference in mean in-plane Ru-O bond length relative to the value in the high temperature structure of Ca_2RuO_4 as imposed through x_0+y_0 where $x_0=y_0$

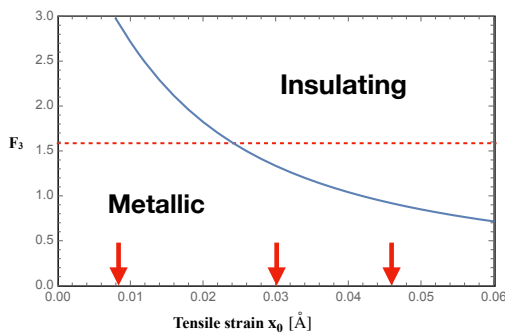


FIG. 13: Phase diagram of epitaxially constrained Ca_2RuO_4 in plane of tensile strain (defined as difference of mean in-plane Ru-O bond length from value in the high temperature structure) in \AA and coupling parameter F_3 . Red dashed line: value of F_3 at which metal insulator transition occurs in bulk system. Arrows (red on line) indicate strain imposed by epitaxial growth on (from left to right) LaAlO_3 , NSAT and NdGaO_3 ; NdAlO_3 corresponding to tensile strain is not shown.

and

$$z^* = (x_0 + y_0) \left(\frac{1 + \sqrt{2}\lambda_0}{2 - \sqrt{2}\lambda_0} + \frac{K_{00} - K_{33} + \frac{K_{30}}{\sqrt{2}}}{2K_{33} + 2\sqrt{2}K_{30} + K_{00}} \right) \quad (17)$$

The epitaxial constraint thus has three effects: it increases the net stiffness to lattice distortions by preventing relaxations of the lattice coordinates associated with in-plane bond lengths, making the insulating phase more difficult to obtain. Second, it reduces the electron lattice coupling (Eq. 16) which also makes it more difficult to obtain an insulating phase. Finally, it provides a term linearly proportional to ΔN , which for positive epitaxial strain favors the insulating phase. The left panel of Fig. 12 shows the change in apical Ru-O bond length as a function of epitaxial strain; the right hand panel the occupancy difference ΔN . The first order transition is evident. Note that for an epitaxial strain matching the

in-plane lattice constant of the high temperature metallic phase, insufficient lattice energy is available to stabilize the insulating phase. As the tensile strain is increased, the octahedral deformation, which couples linearly to ΔN , increases, and beyond a critical value drives a first order transition.

Experiments (Ref [59, 60]) have studied films grown epitaxially on substrates NdAlO_3 , LaAlO_3 , NSAT and NdGaO_3 corresponding to changes (relative to the high-T state, and assuming the Ru-O bond length exactly tracks the in-plane strain) in average in-plane Ru-O lattice parameters of -0.04\AA , 0.008\AA , 0.03\AA and 0.046\AA respectively. Fig. 13 shows that the theory, with no adjustable parameters, predicts that for the theoretically predicted coupling $F_3 = 2.8\text{eV}/\text{\AA}$ the films grown on NdAlO_3 and LaAlO_3 should be metallic, while the films grown on NSAT and NdGaO_3 should be insulating. In the experiment the LaAlO_3 -strained material has a transition at $T \approx 200\text{K}$ from a high temperature metal to a low temperature weak insulator/bad metal, while the others are metallic and insulating as predicted by the theory. The qualitative agreement is good; the quantitative discrepancies may arise from a more subtle relation between Ru-O bond length and in plane lattice constant than was assumed in Ref [7] or from small systematic errors in the theory. The good correspondence between experiment and theory show the utility of the methodology introduced here.

V. TEMPERATURE DEPENDENCE

The methods presented here provide some insight into the physics of the temperature-driven metal-insulator

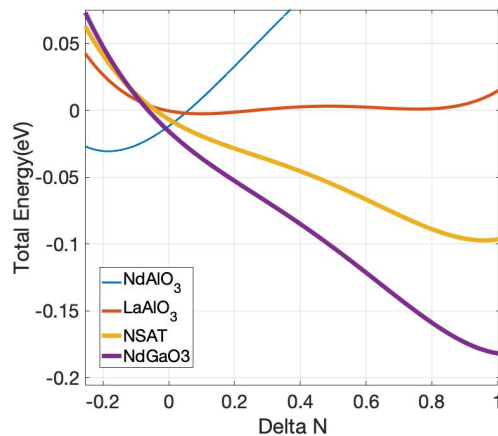


FIG. 14: Total energy plotted against orbital disproportionation ΔN for materials grown on four substrates indicated in the legend which provide different strains relative to the metallic phase of Ca_2RuO_4 . For tensile strain (NdAlO_3), the material is always metallic and the orbital polarization has the opposite sign from in the insulating state.

Temperature	χ_0^{-1} (eV)	β (eV)	γ (eV)
387K	0.0937	-0.0781	0.0519
580K	0.0811	-0.0427	0.0346
773K	0.0773	-0.0197	0.0227
966K	0.0806	-0.0082	0.0172

TABLE III: Parameters that characterize the temperature dependence of the electronic energy as extracted by fitting the temperature dependent electronic free energy data presented in Fig. 15

transition, indicating an important area for future research. We see from Figs. 4 and 7 that for the nickelates the low T energy landscape is characterized by two minima, with energy differences ranging from 80 meV (LuNiO₃) to 25 meV (NdNiO₃). In the nickelates, as the temperature increases a first order metal-insulator transition occurs. The lattice distortion Q exhibits negligible temperature dependence over the entire insulating phase, indicating that the minima remain robust and the transition is driven by an entropic effect that lifts up the free energy of the large ΔN extremum relative to that of the $\Delta N = 0$ extremum.

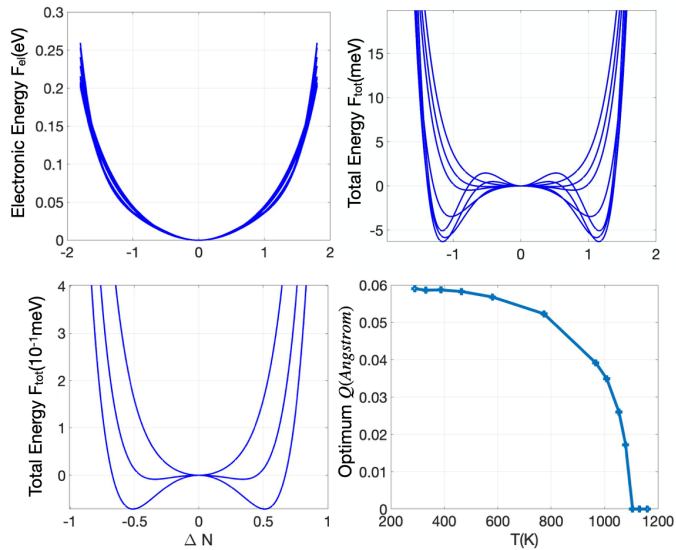


FIG. 15: Upper left panel: electronic free energy as function of electronic disproportionation ΔN computed for NdNiO₃ at temperatures from 290K to 1200K. Upper right panel: total free energy computed for bulk NdNiO₃ for temperatures of $T=290\text{K}$, 387K, 580K, 773K, 967K, 1054K, 1131K. Lower left panel: total expanded view of total free energy for bulk NdNiO₃ at temperatures of 1054K, 1080K, 1105K. Lower Right Panel: Optimal $Q(T)=\Delta N(T)\frac{g}{2K}$

To investigate whether the entropic effect arises from the local correlations captured by the dynamical mean

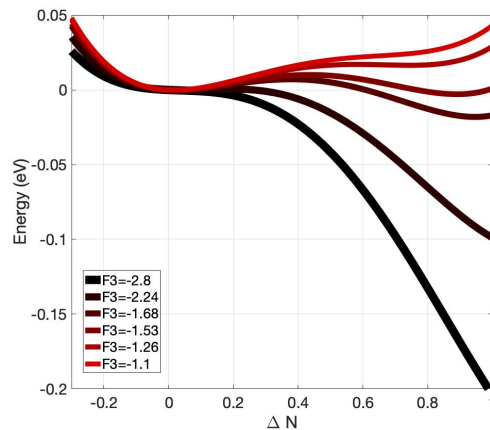


FIG. 16: $F_{total}(\Delta N)$ computed for bulk Ca₂RuO₄ for different values of F_3 .

field approximation, for bulk NdNiO₃ we have extended the calculations shown in Fig. 7 to much higher temperatures by performing calculations with the same methodology and interaction parameters as in [3] but changing the electronic temperature. Fig. 15 shows the results: all of the parameters in the electronic free energy vary systematically with temperature, decreasing in magnitude as the temperature is increased from $\sim 290\text{K}$ to 1000K; the result is a very weakly first order transition at $\approx 1080\text{K}$ (the model actually passes very close to the tricritical point at which the second and fourth order coefficients of the theory simultaneously change sign). This behavior, while theoretically interesting, is inconsistent with the observed strongly first order and much lower transition temperature behavior, suggesting that either the single site dynamical mean field approximation does not adequately describe the temperature dependence of the electronic contribution to the free energy, or that an entropic effect associated with the lattice degrees of freedom plays an important role. Indeed the neglect of spatial fluctuations generically means that single-site DMFT approximations overestimate transition temperatures [61, 62]. It should also be noted that in this material antiferromagnetism plays an important role in the ordering, and that a direct computation [39] of the free energy $F(\Delta N, Q)$ using a different DMFT formalism places paramagnetic NdNiO₃ on the paramagnetic metal side of the transition and yields a stronger low T temperature dependence, and shows for LuNiO₃ a temperature dependence of $F(\Delta N, Q)$ in the range $T < 500\text{K}$ very similar to that found here for NdNiO₃.

Ca₂RuO₄ presents different issues. A substantial temperature dependence is observed [63] across the insulating phase. Since the electronic order parameter ΔN in this material is fixed at its largest possible value for a range of couplings, the temperature dependence must imply a temperature dependence of the electron-lattice coupling F_3 as proposed for related reasons in [7]. Within single-

site dynamical mean field theory, there is no theoretical justification for a strongly temperature-dependent coupling parameter, but on the assumption that changes in electron-lattice coupling F_3 are a proxy for changes in temperature we show in Fig. 16 the energy computed for different values of F_3 . We see that a first order transition occurs at an $F_3 \approx 1.58 \approx 0.6$ of the F_3 we estimated from the low temperature calculation. The phase diagram presented in Fig. 13 then indicates that films grown on substrates with a tensile epitaxial constraint exhibit significantly higher transition temperatures than found in bulk, roughly consistent with experiment.

VI. DISCUSSION AND OUTLOOK

This paper has analysed metal-insulator transitions in quantum materials by constructing an energy functional $F(\Delta N, Q)$ that depends on suitably defined electronic (ΔN) and lattice (Q) order parameters. The first assumption enabling the construction is that the lattice energy is quadratic in deviations from an equilibrium position at fixed value of the electron order parameter, in other words that the physics controlling the relevant atomic force constants arises from chemical bonds inside the solid that are only weakly affected by the transition from metal to insulator. This and the harmonic nature of the lattice response are found in density functional calculations (see e.g. the supplementary material of Ref. [3]) and are further supported by the observation that phonon frequencies do not change much across the transitions of interest. The second assumption is that the coupling between electronic and lattice degrees of freedom is linear, and may be determined a-priori. This second assumption has been confirmed by explicit calculations (see, for example, the supplementary information in [3]). Further investigation of these assumptions, and identification of compounds in which they break down, is an important topic for future research. One important direction is a detailed comparison of results obtained along the lines indicated here to direct computations of energies and free energies [39, 57, 58, 64]

Given these assumptions, a many-body calculation of electronic configuration as a function of lattice distortion may be used to construct free energies, essentially by integrating the equation of state. We accomplish the integration by fitting the equation of state results to a polynomial which is integrated analytically. This procedure avoids ambiguities associated with the coexistence region of the first order transition.

We applied the methodology to two currently interesting families of compounds, that exhibit first order metal-insulator transitions as the temperature is decreased: the rare earth perovskite nickelates $RNiO_3$, and Ca_2RuO_4 . The transition in the $RNiO_3$ is a symmetry breaking transition leading to two inequivalent Ni sites and an alternating pattern of long and short Ni-O bond lengths. The transition in Ca_2RuO_4 is isosymmetric, with no bro-

ken crystal symmetries. In both materials, we find that if the lattice coordinate is set to the value appropriate to the high temperature metallic state, the resulting energy $F(\Delta N, Q = 0)$ has only one minimum, at $\Delta N = 0$. It is only after the coupling to the lattice is included that the total functional $F(\Delta N, Q)$ acquires a minimum at a $\Delta N, Q \neq 0$. We therefore conclude that lattice effects are essential in driving the metal-insulator transition in both compounds, rather than being merely a minor consequence of a fundamentally electronically driven transition, thereby settling a long-standing controversy. It is important to note however that although the purely electronic theory does not produce a metal-insulator transition, the correlation contribution to the electronic energy is still important and calculations on a beyond-DFT level are apparently required to obtain correct energetics.

It is important to consider the limitations of our conclusions. First, while the approach introduced here will work with any method that calculates the electronic order parameter as a function of lattice distortion $\Delta N(Q)$, in practice the information available in the literature comes from the density functional plus dynamical mean field methodology. While this method successfully produces results that are consistent with many experiments, its precise quantitative accuracy is unknown. The method does require an identification of correlated orbitals, it relies on the assumption that density functional theory gives an adequate account of the energetics of the uncorrelated orbitals, it requires specification of interaction parameters, and its solution of the many body problem involves a stringent locality assumption. Cross checking via other methods (as for example was done for Ca_2RuO_4 in Ref. [65]) would be desirable. Further, there are several variants of the DMFT plus DFT methodology, differing the choice of energy window and the representation of correlated states [66]; the dependence of our conclusions on the implementation is an interesting question.

The specification of interaction parameters is of particular importance. As shown e.g. in Refs. [35, 49], as the interaction parameters are increased in magnitude, a transition can be generated in the purely electronic theory. The precise statement made here is that with interaction parameters determined by reproducing physical properties including gaps and effective masses, the purely electronic theory does not exhibit a phase transition: electron-lattice coupling plays an essential role in stabilizing the insulating states.

It will also be noted that while the theory presented here reproduces trends and orders of magnitude very well, it has some quantitative deficiencies, for example predicting that $PrNiO_3$ is metallic but close to the phase boundary when in fact it is insulating but close to the phase boundary, with the lowest transition temperature of any bulk member of the $RNiO_3$ nickelate family. This deficiency is likely to be remedied by inclusion of magnetism in the theory, since in $PrNiO_3$ and $NdNiO_3$, but not in the other compounds studied in this paper, the metal-insulator transition is accompanied by a magnetic

transition. Similarly the phase diagram of epitaxially constrained Ca_2RuO_4 films is qualitatively correct but exhibits quantitative discrepancies with experiment. We note that in this paper no attempt was made to adjust the parameters from the literature or to fine-tune the fits to obtain better agreement with experiment. Small changes, reflecting moderate parameter uncertainties and modest systematic errors in the DFT+DMFT approach, would likely cure these discrepancies.

The access to the free energy provided by our methods enables additional insights. Issues relating to temperature dependence were discussed in Section V. The energy landscape shown in Fig. 1 makes it clear that only one narrowly defined path connects the metallic and insulating minima; this information may be used to investigate the kinetics of order parameter nucleation if the material is supercooled or superheated across the phase boundary. Further, the differing roles of the electronic and lattice degrees of freedom in defining the energy landscape make possible an analysis of the kinetics of state evolution after excitation. For example, excitation might rapidly heat the electrons (leading to changes in F_{el}) but only slowly heat the lattice degrees of freedom (which would in any event respond more slowly). Extension of the theory presented here to include the antiferromagnetism that occurs in the rare earth nickelates may help understand recent ultrafast experiments exploring the relation between antiferromagnetism, lattice distortions and metallicity in NdNiO_3 [67, 68].

The methods can be applied to quantify the importance of lattice effects in other systems of current interest, including CaFeO_3 [69, 70] which exhibits charge ordering and lattice disproportionation, perovskite titanates and vanadates, where lattice distortions couple to orbital ordering

[71–73], VO_2 where a dimerization instability occurs [74], V_2O_3 where the metal-insulator transition couples to the volume of the material [75], and the rare earth manganites where electronic charge, orbital and magnetic ordering are tightly coupled to lattice distortions [76, 77]. We also observe that while we presented results based on dynamical mean field calculations, the method is generic in nature and can easily be used with other electronic structure methods, including DFT, DFT+U, Gutzwiller[78, 79], Auxiliary-Boson[80–83] - particularly with the advent of new codes that calculate energy and naturally handle symmetry breaking[84–87], DFT+U[88, 89], and quantum Monte Carlo[90].

ACKNOWLEDGMENTS

We are indebted to Antoine Georges and Oleg Peil for inspiration, helpful comments and advice at various stages of this work. Discussions with Jennifer Fowlie, Claribel Dominguez, Bernat Mundet Bolos, Marta Gibert, and Jean-Marc Triscone stimulated this project. We would also like to acknowledge suggestions to improve this manuscript from Lauren Walters, Sophie Beck, Alexander Hampel, Claribel Dominguez, as well as conversations with James Rondinelli, Kyle Miller and Danilo Puggioni during the preparation of this manuscript. ABG was partly supported by the Advanced Research Projects Agency-Energy (ARPA-E), U.S. Department of Energy, under Award Number DE-AR0001209. The views and opinions of authors expressed herein do not necessarily state or reflect those of the United States Government or any agency thereof. The Flatiron Institute is a division of the Simons Foundation.

-
- [1] M. Imada, A. Fujimori, and Y. Tokura, Metal-insulator transitions, *Reviews of Modern Physics* **70**, 1039 (1998).
 - [2] C. Domínguez, A. B. Georgescu, B. Mundet, Y. Zhang, J. Fowlie, A. Mercy, A. Waelchli, S. Catalano, D. T. Alexander, P. Ghosez, A. Georges, A. J. Millis, M. Gibert, and J. M. Triscone, Length scales of interfacial coupling between metal and insulator phases in oxides, *Nature Materials* **19**, 1182 (2020).
 - [3] A. B. Georgescu, O. E. Peil, A. S. Disa, A. Georges, and A. J. Millis, Disentangling lattice and electronic contributions to the metal-insulator transition from bulk vs. Layer confined RNiO_3 , *Proceedings of the National Academy of Sciences of the United States of America* **116**, 14434 (2019).
 - [4] O. E. Peil, A. Hampel, C. Ederer, and A. Georges, Mechanism and control parameters of the coupled structural and metal-insulator transition in nickelates, *Physical Review B* **99**, 245127 (2019).
 - [5] A. S. Disa, A. B. Georgescu, J. L. Hart, D. P. Kumah, P. Shafer, E. Arenholz, D. A. Arena, S. Ismail-Beigi, M. L. Taheri, F. J. Walker, and C. H. Ahn, Control of hidden ground-state order in NdNiO_3 Superlattices, *Physical Review Materials* **1**, 024410 (2017).
 - [6] N. J. Szymanski, L. N. Walters, D. Puggioni, and J. M. Rondinelli, Design of Heteroanionic MoON Exhibiting a Peierls Metal-Insulator Transition, *Physical Review Letters* , 236402 (2019).
 - [7] Q. Han and A. Millis, Lattice Energetics and Correlation-Driven Metal-Insulator Transitions: The Case of Ca_2RuO_4 , *Physical Review Letters* **121**, 67601 (2018).
 - [8] E. C. Schueller, K. D. Miller, W. Zhang, J. L. Zuo, J. M. Rondinelli, S. D. Wilson, and R. Seshadri, Structural signatures of the insulator-to-metal transition in $\text{BaCo}_{1-x}\text{Ni}_x\text{S}_2$, *Physical Review Materials* , 104401 (2020).
 - [9] Y. Qi and K. M. Rabe, Electron-lattice coupling contributions to polarization switching in charge-order-induced ferroelectrics, <http://arxiv.org/abs/2103.16466> (2021).
 - [10] A. Mercy, J. Bieder, J. Iniguez, and P. Ghosez, Structurally triggered metal-insulator transition in rare-earth nickelates, *Nature Communications* **8**, 1677 (2017).
 - [11] S. Catalano, M. Gibert, J. Fowlie, J. Iniguez, J. M. Triscone, and J. Kreisel, Rare-earth nickelates RNiO_3 : Thin films and heterostructures, *Reports on Progress in Physics* **81**, 046501 (2018).

- [12] S. Ismail-Beigi, F. J. Walker, A. S. Disa, K. M. Rabe, and C. H. Ahn, *Picoscale materials engineering* (2017).
- [13] A. V. Boris, Y. Matiks, E. Benckiser, A. Frano, P. Popovich, V. Hinkov, P. Wochner, E. Detemple, V. K. Malik, C. Bernhard, T. Prokscha, A. Suter, Z. Salman, E. Morenzoni, G. Cristiani, H. Habermeier, and B. Keimer, Dimensionality Control of Electronic Phase Transitions in Nickel-Oxide Superlattices, *Science Reports* **332**, 937 (2011).
- [14] D. P. Kumah, A. S. Disa, J. H. Ngai, H. Chen, A. Malashevich, J. W. Reiner, S. Ismail-Beigi, F. J. Walker, and C. H. Ahn, Tuning the structure of nickelates to achieve two-dimensional electron conduction, *Advanced Materials* **26**, 1935 (2014).
- [15] S. Middey, D. Meyers, M. Kareev, Y. Cao, X. Liu, P. Shafer, J. W. Freeland, J. W. Kim, P. J. Ryan, and J. Chakhalian, Disentangled Cooperative Orderings in Artificial Rare-Earth Nickelates, *Physical Review Letters* **120**, 156801 (2018).
- [16] A. X. Gray, A. Janotti, J. Son, J. M. Lebeau, S. Ueda, Y. Yamashita, K. Kobayashi, A. M. Kaiser, R. Sutarto, H. Wadati, G. A. Sawatzky, C. G. Van De Walle, S. Stemmer, and C. S. Fadley, Insulating state of ultrathin epitaxial LaNiO₃ thin films detected by hard x-ray photoemission, *Physical Review B - Condensed Matter and Materials Physics* **84**, 1 (2011).
- [17] S. Stemmer and A. J. Millis, Quantum confinement in oxide quantum wells, *MRS Bulletin* **38**, 1032 (2013).
- [18] P. J. Phillips, X. Rui, A. B. Georgescu, A. S. Disa, P. Longo, E. Okunishi, F. Walker, C. H. Ahn, S. Ismail-Beigi, and R. F. Klie, Experimental verification of orbital engineering at the atomic scale: Charge transfer and symmetry breaking in nickelate heterostructures, *Physical Review B* **95**, 205131 (2017).
- [19] M. Kotiuga and K. M. Rabe, High-density electron doping of SmNiO₃ from first principles, *Physical Review Materials* **3**, 115002 (2019).
- [20] J. Y. Zhang, H. Kim, E. Mikheev, A. J. Hauser, and S. Stemmer, Key role of lattice symmetry in the metal-insulator transition of NdNiO₃ films, *Scientific Reports* **6**, 23652 (2016).
- [21] J. Shamblyn, M. Heres, H. Zhou, J. Sangoro, M. Lang, J. Neufeind, J. A. Alonso, and S. Johnston, Experimental evidence for bipolaron condensation as a mechanism for the metal-insulator transition in rare-earth nickelates, *Nature Communications* **9**, 86 (2018).
- [22] D. Meyers, J. Liu, J. W. Freeland, S. Middey, M. Kareev, J. Kwon, J. M. Zuo, Y. D. Chuang, J. W. Kim, P. J. Ryan, and J. Chakhalian, Pure electronic metal-insulator transition at the interface of complex oxides, *Scientific Reports* **6**, 27934 (2016).
- [23] M. Först, K. R. Beyerlein, R. Mankowsky, W. Hu, G. Mattoni, S. Catalano, M. Gibert, O. Yefanov, J. N. Clark, A. Frano, J. M. Glowina, M. Chollet, H. Lemke, B. Moser, S. P. Collins, S. S. Dhesi, A. D. Caviglia, J. M. Triscone, and A. Cavalleri, Multiple Supersonic Phase Fronts Launched at a Complex-Oxide Heterointerface, *Physical Review Letters* **118**, 027401 (2017).
- [24] M. Först, A. D. Caviglia, R. Scherwitzl, R. Mankowsky, P. Zubko, V. Khanna, H. Bromberger, S. B. Wilkins, Y. D. Chuang, W. S. Lee, W. F. Schlotter, J. J. Turner, G. L. Dakovski, M. P. Minitti, J. Robinson, S. R. Clark, D. Jaksch, J. M. Triscone, J. P. Hill, S. S. Dhesi, and A. Cavalleri, Spatially resolved ultrafast magnetic dynamics initiated at a complex oxide heterointerface, *Nature Materials* **14**, 883 (2015).
- [25] M. Medarde, P. Lacorre, K. Conder, F. Fauth, and A. Furrer, Giant ¹⁶O-¹⁸O Isotope Effect on the Metal-Insulator Transition of RNiO₃ Perovskites (R=Rare Earth), *Physical Review Letters* **80**, 2397 (1998).
- [26] W. Hu, S. Catalano, M. Gibert, J. M. Triscone, and A. Cavalleri, Broadband terahertz spectroscopy of the insulator-metal transition driven by coherent lattice deformation at the SmNiO₃/LaAlO₃ interface, *Physical Review B* **93**, 161107(R) (2016).
- [27] A. D. Caviglia, M. Först, R. Scherwitzl, V. Khanna, H. Bromberger, R. Mankowsky, R. Singla, Y. D. Chuang, W. S. Lee, O. Krupin, W. F. Schlotter, J. J. Turner, G. L. Dakovski, M. P. Minitti, J. Robinson, V. Scagnoli, S. B. Wilkins, S. A. Cavill, M. Gibert, S. Gariglio, P. Zubko, J. M. Triscone, J. P. Hill, S. S. Dhesi, and A. Cavalleri, Photoinduced melting of magnetic order in the correlated electron insulator NdNiO₃, *Physical Review B - Condensed Matter and Materials Physics* **88**, 220401(R) (2013).
- [28] G. Guzman-Verri, R. Brierley, and P. Littlewood, Elastic interactions and control of the Mott transition, *arXiv:1701.02318* (2017).
- [29] B. Mandal, S. Sarkar, S. K. Pandey, P. Mahadevan, C. Franchini, A. J. Millis, and D. D. Sarma, The driving force for charge ordering in rare earth nickelates, *arXiv:1701.06819* (2017).
- [30] H. Park, A. J. Millis, and C. A. Marianetti, Influence of quantum confinement and strain on orbital polarization of four-layer LaNiO₃ superlattices: A DFT+DMFT study, *Physical Review B* **93**, 1 (2016).
- [31] J. Ruppen, J. Teyssier, O. E. Peil, S. Catalano, M. Gibert, J. Mravlje, J. M. Triscone, A. Georges, and D. Van Der Marel, Optical spectroscopy and the nature of the insulating state of rare-earth nickelates, *Physical Review B - Condensed Matter and Materials Physics* **92**, 155145 (2015).
- [32] O. E. Peil, M. Ferrero, and A. Georges, Orbital polarization in strained LaNiO₃: Structural distortions and correlation effects, *Physical Review B - Condensed Matter and Materials Physics* **90**, 045128 (2014).
- [33] M. J. Han, X. Wang, C. A. Marianetti, and A. J. Millis, Dynamical mean-field theory of nickelate superlattices, *Physical Review Letters* **107**, 206804 (2011).
- [34] P. Seth, O. E. Peil, L. Pourvorskii, M. Betzinger, C. Friedrich, O. Parcollet, S. Biermann, F. Aryasetiawan, and A. Georges, Renormalization of effective interactions in a negative charge transfer insulator, *Physical Review B* **96**, 205139 (2017).
- [35] A. Subedi, O. E. Peil, and A. Georges, Low-energy description of the metal-insulator transition in the rare-earth nickelates, *Physical Review B - Condensed Matter and Materials Physics* **91**, 1 (2015).
- [36] H. U. R. Strand, Valence-skipping and negative-U in the d-band from repulsive local Coulomb interaction, *Physical Review B - Condensed Matter and Materials Physics* **90**, 155108 (2014).
- [37] A. Blanca-Romero and R. Pentcheva, Confinement-induced metal-to-insulator transition in strained LaNiO₃/LaAlO₃ superlattices, *Physical Review B - Condensed Matter and Materials Physics* **84**, 195450 (2011).
- [38] O. Janson and K. Held, Intrinsic temperature phase diagram of (111) nickelate bilayers, *Physical Review B* **98**, 115118 (2018).

- (2018).
- [39] K. Haule and G. L. Pascut, Mott transition and magnetism in rare earth nickelates and its fingerprint on the x-ray scattering, *Nature Scientific Reports* , 10375 (2017).
- [40] S. Koohfar, A. B. Georgescu, A. N. Penn, J. M. Lebeau, E. Arenholz, and D. P. Kumah, Confinement of magnetism in atomically thin $\text{La}_{0.7}\text{Sr}_{0.3}\text{CrO}_3/\text{La}_{0.7}\text{Sr}_{0.3}\text{MnO}_3$ heterostructures, *npj Quantum Materials* 10.1038/s41535-019-0164-1 (2019).
- [41] S. Koohfar, A. B. Georgescu, I. Hallsteinsen, R. Sachan, M. A. Roldan, E. Arenholz, and D. P. Kumah, Effect of strain on magnetic and orbital ordering of $\text{LaSrCrO}_3 / \text{LaSrMnO}_3$ heterostructures, *Physical Review B* , 64420 (2020).
- [42] P. Zubko, S. Gariglio, M. Gabay, P. Ghosez, and J.-m. Triscone, Interface Physics in Complex Oxide Heterostructures, *Annual Review of Condensed Matter Physics* , 141 (2011).
- [43] Z. Liao, N. Gauquelin, R. J. Green, K. Müller-Caspary, I. Lobato, L. Li, S. Van Aert, J. Verbeeck, M. Huijben, M. N. Grisolia, V. Rouco, R. El Hage, J. E. Villegas, A. Mercy, M. Bibes, P. Ghosez, G. A. Sawatzky, G. Rijnders, and G. Koster, Metal-insulator-transition engineering by modulation tilt-control in perovskite nickelates for room temperature optical switching., *Proceedings of the National Academy of Sciences of the United States of America* , 201807457 (2018).
- [44] S. J. May, C. R. Smith, J. Kim, E. Karapetrova, A. Bhattacharya, and P. J. Ryan, Control of octahedral rotations in $(\text{LaNiO}_3)_n/(\text{SrMnO}_3)_m$ superlattices, , 153411 (2011).
- [45] D. Lee, B. Chung, Y. Shi, N. Campbell, F. Xue, K. Song, J. P. Podkaminer, T. H. Kim, P. J. Ryan, T. R. Paudel, J. W. Spinuzzi, D. A. Tenne, E. Y. Tsymlal, M. S. Rzchowski, L. Q. Chen, J. Lee, and C. B. Eom, Isostructural metal-insulator transition in VO_2 , *Science* , 1037 (2018).
- [46] A. Charnukha, G. X. Ni, P. Radhakrishnan, M. Minola, A. Pasupathy, A. V. Boris, and E. Benckiser, Coexisting first and second order electronic phase transitions in a correlated oxide, **14**, 1056 (2018).
- [47] D. Kartoon, U. Argaman, and G. Makov, Driving forces behind the distortion of one-dimensional monatomic chains: Peierls theorem revisited, *Physical Review B* **98**, 165429 (2018).
- [48] U. Argaman, D. Kartoon, and G. Makov, Distorted structures in half-filled p-band materials, *Journal of Physics Condensed Matter* **31**, 465501 (2019).
- [49] A. B. Georgescu, P. Ren, A. R. Toland, E. A. Olivetti, N. Wagner, and J. M. Rondinelli, A Database and Machine Learning Model to Identify Thermally Driven Metal-Insulator Transition Compounds, [arxiv:2010.13306](https://arxiv.org/abs/2010.13306) (2020).
- [50] Y. Wang, A. Iyer, W. Chen, and J. M. Rondinelli, Featureless adaptive optimization accelerates functional electronic materials design, *Applied Physics Reviews* , 041403 (2020).
- [51] J. H. Chu, H. Kue, J. Analytis, and I. Fisher, Divergent nematic susceptibility in an iron arsenide superconductor, *Science* **337**, 710 (2012).
- [52] P. Lacorre, M. Medarde, M. Zacchigna, M. Grioni, and G. Margaritondo, Electronic-structure evolution through the metal-insulator transition in (formula presented), *Physical Review B - Condensed Matter and Materials Physics* **60**, R8426 (1999).
- [53] J. G. Cheng, J. S. Zhou, J. B. Goodenough, J. A. Alonso, and M. J. Martinez-Lope, Pressure dependence of metal-insulator transition in perovskites R NiO_3 ($\text{R}=\text{Eu}, \text{Y}, \text{Lu}$), *Physical Review B - Condensed Matter and Materials Physics* **82**, 1 (2010).
- [54] B. Chen, N. Gauquelin, R. J. Green, J. H. Lee, C. Piamonteze, M. Spreitzer, D. Jannis, J. Verbeeck, M. Bibes, M. Huijben, G. Rijnders, and G. Koster, Spatially Controlled Octahedral Rotations and Metal-Insulator Transitions in Nickelate Superlattices, *Nano Letters* , 1295 (2021).
- [55] H. Chen, D. P. Kumah, A. S. Disa, F. J. Walker, C. H. Ahn, and S. Ismail-Beigi, Modifying the electronic orbitals of nickelate heterostructures via structural distortions, *Physical Review Letters* **110**, 1 (2013).
- [56] H. Park, A. J. Millis, and C. a. Marianetti, Site-selective Mott transition in rare-earth-element nickelates, *Physical Review Letters* **109**, 156402 (2012).
- [57] H. Park, A. Millis, and C. Marianetti, Total energy calculations using DFT+ DMFT: computing the pressure phase diagram of the rare earth nickelates, *Physical Review B* **89**, 245133 (2014).
- [58] H. Park, A. J. Millis, and C. A. Marianetti, Computing total energies in complex materials using charge self-consistent DFT+DMFT, *Physical Review B - Condensed Matter and Materials Physics* **90**, 1 (2014).
- [59] H. Nair, J. Ruf, Y. Liu, N. Shukla, B. Grisafe, C. Chang, Q. Han, A. Millis, D. Muller, S. Datta, K. Shen, and D. Schlom, No Title, (2017).
- [60] C. Dietl, S. K. Sinha, G. Christiani, Y. Khaydukov, T. Keller, D. Putzky, S. Ibrahimkuty, P. Wochner, G. Logvenov, P. A. Van Aken, B. J. Kim, and B. Keimer, Tailoring the electronic properties of Ca_2RuO_4 via epitaxial strain, *Applied Physics Letters* **112**, 1 (2018).
- [61] M. J. Calderón, L. Brey, and F. Guinea, Surface electronic structure and magnetic properties of doped manganites, *Physical Review B - Condensed Matter and Materials Physics* **60**, 6698 (1999).
- [62] A. Chattopadhyay and A. Millis, Optical spectral weights and the ferromagnetic transition temperature of colossal-magnetoresistance manganites: Relevance of double exchange to real materials, *Physical Review B - Condensed Matter and Materials Physics* **61**, 10738 (2000).
- [63] O. Friedt, M. Braden, G. André, P. Adelman, S. Nakatsuji, and Y. Maeno, Structural and magnetic aspects of the metal-insulator transition in $\text{Ca}_{2-x}\text{Sr}_x\text{RuO}_4$, *Physical Review B* **63**, 1744321 (2001).
- [64] K. Haule, Exact Double Counting in Combining the Dynamical Mean Field Theory and the Density Functional Theory, *Physical Review Letters* **115**, 196403 (2015).
- [65] H. Hao, A. Georges, A. J. Millis, B. Rubenstein, Q. Han, and H. Shi, Metal-insulator and magnetic phase diagram of $\{\text{Ca}\}_{-2}\{\text{RuO}\}_{-4}$ from auxiliary field quantum Monte Carlo and dynamical mean field theory, *Physical Review B* **101**, 235110 (2020).
- [66] J. Karp, A. Hampel, and A. J. Millis, Dependence of DFT+DMFT Results on the Construction of the Correlated Orbitals, <http://arxiv.org/abs/2102.08522> (2021).
- [67] V. Stoica, D. Puggioni, J. Zhang, R. Singla, G. L. Dakovski, G. Coslovich, M. H. Seaberg, M. Kareev, S. Middey, P. Kissin, R. D. Averitt, J. Chakhalian, H. Wen, J. M. Rondinelli, and J. W. Freeland, Disentangling electronic and magnetic order in NdNiO_3 at ultrafast timescales, [arXiv:2004.03694](https://arxiv.org/abs/2004.03694) (2020).
- [68] M. Forst, A. D. Caviglia, R. Scherwitzl, R. Mankowsky,

- P. Zubko, V. Khanna, H. Bromberger, S. B. Wilkins, Y. D. Chuang, W. S. Lee, W. F. Schlotter, J. J. Turner, G. L. Dakovski, M. P. Minitti, J. Robinson, S. R. Clark, D. Jaksch, J. M. Triscone, J. P. Hill, S. S. Dhesi, and A. Cavalleri, Spatially resolved ultrafast magnetic dynamics initiated at a complex oxide heterointerface, *Nature Materials* **14**, 883 (2015).
- [69] P. Woodward, D. Cox, and E. Moshopoulou, Structural studies of charge disproportionation and magnetic order, *Physical Review B - Condensed Matter and Materials Physics* **62**, 844 (2000).
- [70] P. C. Rogge, R. U. Chandrasena, A. Cammarata, R. J. Green, P. Shafer, B. M. Leffler, A. Huon, A. Arab, E. Arenholz, H. N. Lee, T. L. Lee, S. Nemšák, J. M. Rondinelli, A. X. Gray, and S. J. May, Electronic structure of negative charge transfer CaFeO₃ across the metal-insulator transition, *Physical Review Materials* **2**, 015002 (2018).
- [71] E. Pavarini, S. Biermann, A. Poteryaev, A. I. Lichtenstein, A. Georges, and O. K. Andersen, Mott transition and suppression of orbital fluctuations in orthorhombic 3d1 perovskites, *Physical Review Letters* **92**, 176403 (2004).
- [72] S. Beck and C. Ederer, Tailoring interfacial properties in CaVO₃ thin films and heterostructures with SrTiO₃ and LaAlO₃: A DFT+DMFT study, *Physical Review Materials* **4**, 125002 (2020).
- [73] X. J. Zhang, E. Koch, and E. Pavarini, Origin of orbital ordering in YTiO₃ and LaTiO₃, *Physical Review B* **102**, 035113 (2020).
- [74] J. M. Tomczak and S. Biermann, Effective band structure of correlated materials: The case of VO₂, *Journal of Physics Condensed Matter* **19**, 365206 (2007).
- [75] I. Leonov, V. I. Anisimov, and D. Vollhardt, Metal-insulator transition and lattice instability of paramagnetic V₂O₃, *Physical Review B - Condensed Matter and Materials Physics* **91**, 1 (2015).
- [76] S. Uhlenbruck, R. Teipen, R. Klingeler, B. Büchner, O. Friedt, M. Hücker, H. Kierspel, T. Niemöller, L. Pinsard, A. Revcolevschi, and R. Gross, Interplay between charge order, magnetism, and structure in La_{0.875}Sr_{0.125}MnO₃, *Physical Review Letters* **82**, 185 (1999).
- [77] A. S. McLeod, J. Zhang, M. Q. Gu, F. Jin, G. Zhang, K. W. Post, X. G. Zhao, A. J. Millis, W. B. Wu, J. M. Rondinelli, R. D. Averitt, and D. N. Basov, Multimessenger nanoprobe of hidden magnetism in a strained manganite, *Nature Materials* **19**, 397 (2020).
- [78] X. Deng, L. Wang, X. Dai, and Z. Fang, Local density approximation combined with Gutzwiller method for correlated electron systems: Formalism and applications, *Physical Review B - Condensed Matter and Materials Physics* **79**, 075114 (2009).
- [79] K. M. Ho, J. Schmalian, and C. Z. Wang, Gutzwiller density functional theory for correlated electron systems, *Physical Review B - Condensed Matter and Materials Physics* **77**, 1 (2008).
- [80] B. Lau and A. J. Millis, Theory of the Magnetic and Metal-Insulator Transitions in RNiO₃ Bulk and Layered Structures, *Physical Review Letters* **110**, 126404 (2013).
- [81] L. de' Medici and M. Capone, Modeling Many-Body Physics with Slave-Spin Mean-Field: Mott and Hund's Physics in Fe-Superconductors [10.1007/978-3-319-56117-2_4](https://arxiv.org/abs/10.1007/978-3-319-56117-2_4) (2017).
- [82] S. Florens and A. Georges, Slave-rotor mean-field theories of strongly correlated systems and the Mott transition in finite dimensions, *Physical Review B* **70**, 035114 (2004).
- [83] A. B. Georgescu and S. Ismail-Beigi, Generalized slave-particle method for extended Hubbard models, *Physical Review B* **92**, 235117 (2015).
- [84] B. Subsidiary, S. Boss, A. B. Georgescu, M. Kim, and S. Ismail-beigi, Boson Subsidiary Solver (BoSS) v1.1, *Computer Physics Communications* **265**, 107991 (2021).
- [85] A. B. Georgescu and S. Ismail-Beigi, Symmetry breaking in occupation number based slave-particle methods, *Physical Review B* **96**, 165135 (2017).
- [86] A. K. Maurya, M. T. H. Sarder, and A. Medhi, Mott transition, magnetic and orbital orders in the ground state of the two-band Hubbard model using variational slave-spin mean field formalism, <http://arxiv.org/abs/2104.13027> (2021).
- [87] S. R. Hassan and L. DeMedici, Slave spins away from half filling: Cluster mean-field theory of the Hubbard and extended Hubbard models, *Physical Review B* **81**, 035106 (2010).
- [88] V. I. Anisimov, J. Zaanen, and O. K. Andersen, Band theory and Mott insulators: Hubbard U instead of Stoner I, *Physical Review B* **44**, 943 (1991).
- [89] V. I. Anisimov, F. Aryasetiawan, and A. Liechtenstein, First-principles calculations of the electronic structure and spectra of strongly correlated systems: the LDA + U method, *Journal of Physics: Condensed Matter* **9**, 767 (1997).
- [90] M. Jarrell, Hubbard Model in Infinite Dimensions: A QMC Study, *Phys. Rev. Lett.* **69**, 168 (1992).